Design of a Magnetic Field-Controlled Chromatography Process for Efficient and Selective Fractionation of Rare Earth Phosphors from End-of-Life Fluorescent Lamps

Laura Kuger* and Matthias Franzreb

ABSTRACT: Rare earth-containing materials are essential for a wide range of modern technologies and have significant technological and economic importance. Therefore, the development of efficient separation and purification processes for these materials is crucial for environmental sustainability and resource conservation. In this study, we investigated the potential of magnetic field-controlled chromatography for the fractionation of different rare earth-containing phosphors from end-of-life fluorescent lamps. The results demonstrate that with the intrinsic magnetization of the phosphor particles and a careful choice of process parameters, we can control the separation outcome. An optimized gradient shape resulted in purities of up to 95.3% at recoveries of 93.6% ($LaPO_4:Ce^{3+},Tb^{3+}$). The aqueous eluent consumption was found to be quite modest at 4.1 L/g, and it contained only minimal quantities of nontoxic and biodegradable solvent. This study could have significant implications for the development of efficient and effective purification processes for rare earth-containing materials, which are primarily driven by economic concerns and environmental considerations. The possibility of scaling up the process by increasing the column size or transferring it to continuous processing methods could further enhance its practical applicability in industry.

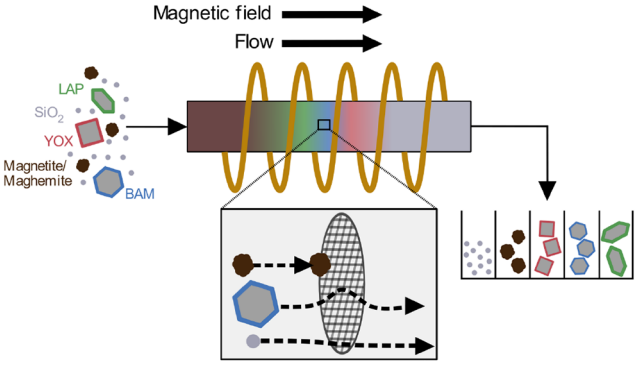

KEYWORDS: *fractionation, separation, chromatography, recycling, rare earth phosphors, magnetics*

1. INTRODUCTION

Rare earths (REs) are a set of 17 elements that have distinct magnetic, electrical, and optical characteristics, making them crucial ingredients in many modern technologies.[1] Numerous high-tech products rely on RE-containing components to function properly, including smartphones, electric vehicles, and renewable energy systems. Increasing efforts to develop more sustainable, low-carbon economies through the implementation of innovative products and technologies have resulted in a flourishing popularity of RE-containing parts.[2] This again substantiates the rapidly increasing demand for REs in recent years.[3,4] However, the scarcity of REs has raised economic concerns. RE markets are known for their volatility, with only a few countries being the main global suppliers.[5−8] Concurrently, these countries possess the most substantial deposits of RE-containing minerals and ores, with China, Brazil, Vietnam, and Russia together accounting for more than 82% of total global reserves.[6] This has caused concerns about other countries' abilities to meet their future needs for these critical commodities. One aspect of diversifying the supply sources and reducing the dependencies is the recycling of RE-containing end-of-life (EOL) products on a large scale. Recycling RE-containing parts can help to stabilize RE prices, making them more accessible to industry and reducing the economic concerns associated with their limited supply. Also, it can help to reduce the environmental impact of RE mining and extraction, which is becoming an increasingly serious issue in the face of the growing demand for these materials.[9]

Although large-scale recycling of RE-containing EOL goods offers huge promise in terms of economic and environmental benefits, it remains a major problem for three key reasons, beginning with the heterogeneous nature of many EOL products, which complicates the recovery of REs in an efficient and cost-effective manner. The remnants of destroyed EOL fluorescent lamp tubes, for instance, usually contain a significant amount of small glass particles due to the destruction procedure, resulting in a substantial reduction in value as well as reusability and making separation difficult,

expensive and time-consuming.[10] Second, the small amounts of REs present in EOL products often make the recycling process uneconomical. The expenses for collecting, dismantling, and processing the products often outweigh the value of the recovered REs.[11] Third, a lack of incentives,[12] adequate infrastructure, and logistics routes for recycling REs from EOL products are also huge obstacles.[13]

Despite the challenges of recycling RE-containing EOL products on a large scale, recovering phosphor particles from fluorescent lamp waste has been the focus of several studies. The luminous color of a fluorescent lamp is determined by the composition of the phosphor mixture used. Various compounds emitting at different wavelengths are typically combined to create this mixture, such as red europium-doped yttrium oxide (YOX), blue europium-doped barium magnesium aluminate (BAM), and green cerium/terbium-doped lanthanum phosphate (LAP). However, according to Binnemans et al., the total amount of these phosphor particles constitutes only 0.3 to 0.6%(w/w) of a ground EOL fluorescent lamp.[12] Conversely, the largest portion is diamagnetic glass or plastics, accounting for approximately 93%(w/w) of the total mass. The residual fraction consists of metals (ferromagnetic and paramagnetic, approximately 5%(w/w)) as well as halophosphate phosphors (approximately 1.35%(w/w)) and a very small fraction of mercury (0.005%(w/w)). Several studies have described different approaches to recover RE-containing phosphor particles from EOL fluorescent lamp waste for recycling purposes. Gravity separation is premised on the fact that the densities of different RE-containing phosphors/oxides specifically deviate from each other and from other material types such as iron oxides and silicates.[14] However, the size distributions of the particle collectives can greatly affect the performance of the process and may counteract the effects of density differences. For RE-containing particle types with similar densities, electrostatic separation can be considered, with the disadvantage that the feed material must be completely dry.[15,16] Flotation techniques make use of differences in the surface characteristics of RE-containing particles, such as their surface charge,[17,18] to separate them and are already employed on an industrial scale. Yet, separating lamp phosphor particles through froth flotation can be a challenging task since the different phosphors share similar characteristics with regard to their hydrophobicity. In some cases, no optimal conditions could be found to achieve reasonable recovery and purity.[19] However, alternative methods such as two-liquid flotation have shown promising results.[20−22] Leveraging the distinct magnetic susceptibilities of the phosphors and contaminants as a basis for separation is another effective approach. One example of such a method is magnetic levitation, also known as the Magneto-Archimedes method. This technique combines differences in density and magnetic susceptibility to create a force balance that determines the equilibrium position of each component. This results in characteristic trajectories within a separation chamber, allowing for physical separation on an analytical scale.[23] High-gradient magnetic separation (HGMS) constitutes another method for the separation of paramagnetic materials like RE-containing particles on a larger scale.[24] This principle is based on the strong attractive forces that magnetic particles encounter when placed within a high spatial magnetic field gradient generated by magnetically susceptible wires.[25,26] However, HGMS processes have the drawback that the 'collect-and-elute' character indeed enables capturing of even small magnetic particles, but they are not capable of separating complex mixtures into several fractions in a single processing step. Furthermore, HGMS devices also require a considerable amount of energy because strong magnetic background fields are necessary.[27] Even though, a number of HGMS configurations have already been investigated for their potential for phosphor separation from fluorescent lamps, with some promising outcomes. For instance, Yamashita et al. used HGMS to isolate LAP from a demercurized phosphor mixture from EOL lamps with a background field of 1 T. They chose LAP as the target compound because, among the phosphors in the mixture, it exhibits the highest intrinsic magnetic susceptibility and, hence, magnetic addressability. After repeating the separation three times, they were able to achieve a LAP purity of 87%. However, due to threefold processing, a considerable amount of LAP was discarded, resulting in a total recovery of only 60.7%.[28] The authors also noted that their method is only suitable for the separation of a single phosphor species.[29] In a recent study, Boelens et al. intensively investigated the removal dynamics of multiple fluorescent lamp phosphors in a rotary permanent magnet HGMS system with a horizontal field gradient at a background field of 0.32 T. They observed significant differences in the removal dynamics depending on the phosphor's intrinsic magnetic susceptibilities. Despite this, they concluded that the system was not suitable for phosphor separation in its current configuration, because they found that the removal efficiency declined over time as a result of a shift in the particle size distribution.[30]

Magnetic field superposition has shown to significantly advance ultrafine magnetic particle separation using field flow fractionation (FFF). Initially, microchannels were employed where suspended magnetic particles were externally influenced by a background field, leading to the adherence of the particles to the channel walls.[31,32] In the 1990s, the group of Ohara further explored magnetic FFF by introducing magnetizable bodies, such as wires, into the magnetic background field to amplify the field and improve separation efficiency.[33−35] According to a numerical study conducted by this group, the technique demonstrated potential for separating weakly paramagnetic materials, for instance, neodymium.[34] Also, to label this technique, they have introduced the term *magnetic chromatography* for the first time.[36]

In consideration of the results obtained by the different research groups mentioned above, magnetic chromatography, or more precisely magnetic field-controlled chromatography, may be used to address particles according to their magnetic properties. In this paper, we present an approach based on this technique for the purification of paramagnetic RE-containing phosphors used in EOL fluorescent lamps. Differences in the phosphor's intrinsic susceptibilities[29,30] lead to varying particle affinities towards a magnetizable chromatography matrix. We selectively separated the particle species from each other and from other pollutants within a single processing step by leveraging these affinity differences. Also, the methodology in regard to process optimization is being highlighted, as the main goal of the study was to maximize the purities and recoveries, as well as productivity.

2. AFFINITY MECHANISM

The principle of magnetic field-controlled chromatography relies on the application of a magnetic field and a magnetizable chromatography matrix that amplifies the ambient field. The

magnetic field gradient generated by the matrix affects particles suspended in the liquid as they flow past the stationary chromatography phase. The intensity of this interaction varies depending on the inherent magnetomobility of a given particle type. The impact of various process parameters and particle characteristics on the modulation of particle trajectories is theoretically described below.

A paramagnetic particle with volume V_P and magnetic susceptibility χ is influenced in the vicinity of a cylindrical ferromagnetic single wire with radius r_W when a background magnetic field H_0 is applied and experiences a magnetic force F_m[25,37a]:

$$F_m = V_P \chi H_0 \mu_0 \nabla H \tag{1}$$

with the magnetic field gradient ∇H resulting from the background field H_0 and the wire's specific magnetization M. Assuming that the spherical particle with diameter d_P moves with a viscous liquid flow past the wire under Stokes conditions, it is influenced not only by the magnetic force, but also by a drag force F_d:[26,38]

$$F_d = 3\pi d_P \eta v_{\text{rel}} \tag{2}$$

Here, v_{rel} refers to the velocity difference between the particle and the surrounding fluid and η is the dynamic viscosity of the fluid. The hydrodynamic drag force F_d and the magnetic force F_m counteract each other, resulting in a magnetic velocity, v_m, that describes the effect of the force influences on the particle in an equilibrium state:[39]

$$v_m = \frac{2}{9}\mu_0 \chi M H_0 r_P^2 (\eta r_W)^{-1} \tag{3}$$

Gravitational forces may be neglected depending on the circumstances and the magnitude of the dominating forces.[26] However, given the relatively high densities of the rare earth-doped phosphor materials (>5 g/cm^3) and their large particle diameters of up to 15 μm, this assumption may not hold true in this case. Therefore, to mitigate the impacts of gravitation and buoyancy, the chromatography column was positioned horizontally, with the flow directed from left to right.

Other interactions, such as van der Waals or electrostatic forces, were neglected throughout this study, as both are surface forces. In contrast, forces dependent on the volume of the particles (such as the magnetic force, cf. eq 1) become even more significant in the micrometer size range.[40] Consequently, even moderate external magnetic fields paired with the paramagnetic nature of a particle lead to magnetic force dominance.

Equation 3 suggests that the particle's trajectory is influenced by multiple factors such as fluid viscosity, wire magnetization and radius, as well as particle magnetic susceptibility and radius. This implies that to achieve particle separation, both internal (particle) and external (fluid and geometrical) parameters must be considered. Under constant external conditions, retardation or even total retention of particles with high magnetic susceptibility is expected, while particles with low magnetic susceptibilities would pass the chromatography space with only little or no delay. However, for ultrafine particle collectives (<15 μm or even submicron) with moderate magnetic susceptibilities, magnetic addressing poses a major challenge[25,41] that can only be overcome with the application of high field gradients and deliberate process parameter selection.

3. EXPERIMENTAL SECTION

3.1. External Magnetic Field Source Design. For the generation of an external magnetic field as homogeneous as possible along the entire length L of the chromatography column, a multi-coil arrangement was designed. It consisted of eight individual coils (inner diameter: 28 mm, axial distance: 8 mm, height of one coil: 14 mm) stacked on one another. The coils have been wired in series; therefore, current of the same intensity flowed through them unidirectionally when connecting them to a power supply system (RNDLab, Distrelec Group AG, Nänikon, Switzerland). The winding numbers of the individual coils were optimized in silico by assuming azimuthal symmetry (2D). The integral objective function Q_{int} was minimized by means of a sparse nonlinear optimizer (SNOPT) and by using the multiphysics simulation software COMSOL (version 5.6):

$$Q_{\text{int}} = \int_0^L q(B(n_i))\mathrm{d}z \tag{4}$$

$$q = \frac{1}{L}\left(\frac{B(n_i)}{B_0} - 1\right)^2 \tag{5}$$

B_0 indicates the reference value of the magnetic flux density, and $B(n_i)$ describes the magnetic flux density depending on the single coil's winding numbers n_i, i = 1,2,3,4 (assuming azimuthal and axial symmetry). The winding numbers n_i were set as global control variables, and the coil's geometrical conditions determined the maximum possible number of windings as n = 265, which was, therefore, predefined as an initial value and upper constraint. The lower constraint was set to n = 0.

A comparison between the simulations of an optimized multicoil arrangement and a cylindrical coil (n = 1750), based on equal geometrical premises, can be found in the Supporting Information (SI), Figure S7A. The design and construction of the proposed multicoil arrangement thus provided a more uniform magnetic flux density induced on the central axis than it would have been achievable with a cylindrical coil.

The assembled coil arrangement was characterized by using a Hall probe (FH31, Magnet-Physik Dr. Steingroever GmbH, Cologne, Germany). The measured values and the COMSOL simulation results are compared in Figure S7B. As expected, the induced magnetic flux density showed a linear dependence on the current intensity applied, and a calibration curve was generated, which proved the linear relationship (see Figure S8).

3.2. Chromatography Matrix and Column Packing. In addition to the external magnetic field source detailed above, the type and arrangement of the chromatography matrix elements were as well critical for the profile of the magnetic field gradients within the chromatography space. Materials with high saturation magnetizations and low remanence magnetizations are favorable for magnetism-based fractionation processes due to their ability to induce strong field gradients when exposed to an external magnetic field, yet maintain a relatively weak attraction once the external field is removed. The ferritic stainless steel EN 1.4016 (AISI 430) is an example of such a material, as it has one of the highest saturation magnetization values (M_S = 154.1 Am^{2}kg^{-1}) among all stainless steels and exhibits a very low remanence of only 5.55 Am^{2}kg^{-1}, refer to Figure S4B. Furthermore, its relatively high chromium content of 16% provides good corrosion resistance, which is crucial for use in aqueous media. In order to generate field gradients as defined as possible, woven stainless steel wire meshes (mesh size: 70 μm, wire diameter: 41 μm, Haver & Boecker OHG, Oelde, Germany) were cut out in a circular shape (d = 6.6 mm) and stacked on top of each other within the column. To ensure good permeability, 3D-printed, ring-shaped spacers (d_a = 6.55 mm, h = 100 μm) consisting of perfluoropolyether (PFPE, refer to Kotz et al.[42] for detailed information on the material) were placed between each wire mesh. The PFPE material exhibited good swelling properties, which helped prevent short-circuit flows at the radial extremities of the column due to imprecisely cut wire nets. The chromatography columns used were glass columns with an inner diameter of 6.6 mm and a fixed bed height of 120 mm (Omnifit EZ,

Table 1. Properties of the Particle Collectives Examined Using DLS (Volumetric Median Diameter), AGM (Magnetic Behavior, Normalized Saturation Magnetization, and Magnetic Susceptibility), XRD (Crystal System), and FI (Fluorescence Emission Wavelength)

	median diameter $d_{50,3/}$ nm	magnetic behavior	saturation magnetization M_S/Am^{2}kg^{-1}	magnetic susceptibility χ/-	crystal system	fluorescence emission wavelength at λ_{exc} = 254 nm
SiO_2 nanoparticles (sicastar 50 nm)	63.9	diamagnetic	-	-	-	-
iron oxide nanoparticles (FeO 250 nm)	315.7	ferrimagnetic	48.74	-	-	-
YOX particles	1392.2	paramagnetic	-	0.52×10^{-3}	cubic	613 nm
BAM particles	1430.3	paramagnetic	-	1.19×10^{-3}	hexagonal	451 nm
LAP particles	1382.7	paramagnetic	-	3.69×10^{-3}	monoclinic	544 nm

Diba Industries Inc., Danbury, US). The column's endpieces were equipped with frit filters of 30 μm mesh size. The packed column was filled with ethanol and treated for 15 min in an ultrasonic bath to remove air entrapments. Subsequently, the column was connected to an ÄKTA purifier system (Cytiva, Buckinghamshire, UK) and equilibrated with 20%(v/v) ethanol before performing asymmetry and interstitial volume tests with injections of 1%(v/v) acetone (V = 100 μL). The tests were conducted in duplicate. An asymmetry between 1.0 and 1.6 was considered acceptable, and the column's mean interstitial volume ratios ranged from 53.4% to 56.0%. Refer to the SI for a detailed method description and asymmetry test results (Figure S1 and Table S1).

3.3. Particle Collectives and Analytical Methods. Three different commercially available, RE-doped lamp phosphor particle collectives provided by Leuchtstoffwerk Breitungen GmbH (Breitungen, Germany) were used as paramagnetic components: a cerium/terbium-doped lanthanum phosphate ($LaPO_4$:Ce^{3+},Tb^{3+}, LAP), a europium-doped barium magnesium aluminate ($BaMgAl_{10}O_{17}$:Eu^{2+}, BAM) and an europium-doped yttrium oxide (Y_2O_3:Eu^{3+}, YOX). Iron oxide and silica nanoparticles have been employed as ferrimagnetic and diamagnetic components, respectively (both provided by micromod Partikeltechnik GmbH, Rostock, Germany). Characterization of the particle collectives and their corresponding suspensions was essential to gain insight into the attributes that can influence the performance during fractionation experiments. For details on analytical methodologies and results, the reader is being referred to the SI. In the following, the applied methods are briefly described, and Table 1 summarizes the respective findings.

Investigations on particle size and colloidal stability through dynamic light scattering (DLS) helped to understand particle−particle/particle−milieu interactions, which is particularly relevant for ultrafine and nanoparticles having large surface area-to-volume ratios. The particle size results were verified by an orthogonal method (environmental scanning electron microscopy, ESEM; see Figure 1). Verification of the respective substances and crystal systems was performed using X-ray diffraction (XRD, refer to Figure S3). By revealing the magnetic properties using alternating gradient magnetometry (AGM, see Figure S4), knowledge was acquired about the respective behavior in magnetism-based fractionation processes, as described within this study. Furthermore, it was essential to determine the composition of the particles/suspensions in order to accurately assess the performance of the process operations. Fluorescence spectroscopy was the method of choice for quantitative and qualitative detection of the three RE-containing phosphors, since they are used as phosphorescent components in lamps and therefore emit at specific wavelengths (see Table 1). A linear correlation between concentration and emission counts was found, enabling quantitative detection of the phosphors in suspension (Figure S5). Inductively coupled plasma-optical emission spectrometry (ICP-OES, refer to SI) served as an elemental detection method for silicon and iron, and as an orthogonal validation method for the detection of lanthanum (for LAP), barium and magnesium (for BAM), and yttrium (for YOX).

3.4. Chromatography Fractionation Experiments. A fast protein liquid chromatography (FPLC) system (ÄKTA purifier,

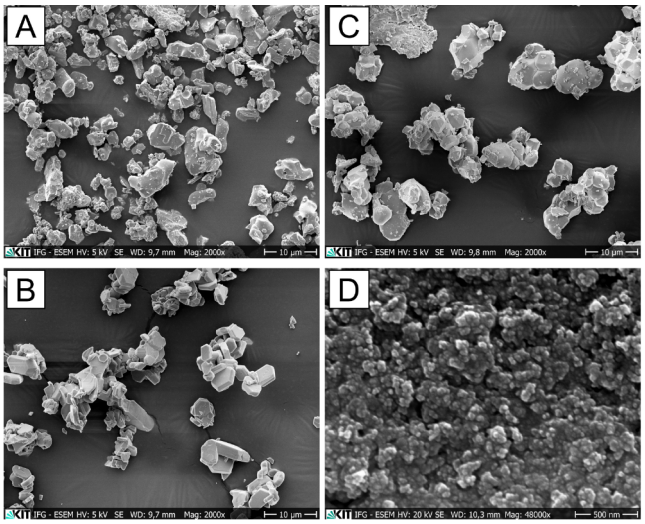

Figure 1. ESEM images of the (A) LAP, (B) BAM, (C) YOX (2000× magnification), and (D) iron oxide (48,000× magnification) particle systems. The operating voltage was set to 5 kV (LAP, BAM, YOX) or 20 kV (iron oxide), and secondary electrons were detected.

Cytiva, UK) equipped with poly(ether ether ketone) (PEEK) tubings was used for conducting the fractionation experiments. The system's dead volume was determined to 0.28 mL via 1% (v/v) acetone injections without a column connected to the system. Figure 2 shows a schematic flowchart of the magnetic field-controlled chromatography process. The mobile phase (20%(v/v) ethanol) was pumped into the system, and injection pulses (V = 0.5 mL) were added to the fluid stream via an injection loop and valve. The mobile phase including the injected particle suspension flowed onto the column, which was surrounded by the external magnetic field source. The

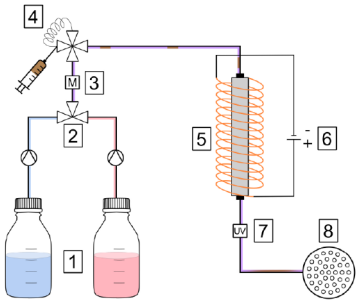

Figure 2. Schematic flow diagram of the magnetic field-controlled chromatography process. (1) eluent reservoirs, (2) three-way valve and eluent mixing point, (3) mixer, (4) injection loop and valve, (5) chromatography column, surrounded by a multi-coil arrangement for magnetic field generation, (6) laboratory power supply system, (7) in-line UV/vis measurement cell, (8) fraction collector.

effluent was collected and divided into individual vessels (V = 0.5 mL) at the column outlet. The process was monitored using an online UV/vis cell at 280 nm.

Different feed compositions were used in this study. For the initial single substance experiments with LAP, BAM, or YOX, the concentrations were 0.1 g/L each. The investigation of phosphor mixtures was conducted using a total concentration of 0.3 g/L, with the three phosphor species LAP, BAM, and YOX each present in equal mass fractions, i.e., with 0.1 g/L each. The composition of the artificial EOL product was roughly based on the composition of ground fluorescent tubes, as reported by Binnemans et al.[12] Specifically, the product mixture consisted of silica particles with a concentration of 13.2 g/L, an iron oxide particle concentration of 0.75 g/L, and a total phosphor concentration of 0.27 g/L, which was evenly distributed among the three phosphor species LAP, BAM, and YOX (c_i = 0.09 g/L).

Three distinct operation modes were investigated and evaluated regarding their fractionation performances throughout the study. During the isocratic chromatography experiments, a constant magnetic flux density (20 mT) and flow rate (1.2 mL/min) was maintained throughout the whole experiment. For the elution mode, the flow rate was set to 1.2 mL/min, the external magnetic field was switched on initially and set to 20 mT, the feed suspension was injected into the system, and the first UV signal peak was observed. Afterward, the external magnetic field was switched off, and the flow rate was simultaneously increased to 5 mL/min, inducing a second peak. For the temporal gradient mode, the flow rate was set to 1.2 mL/min and the external magnetic field was initially set to 50 mT. The feed suspension was injected into the system, and subsequently, the magnetic flux density was reduced stepwise by 5 mT every 0.5 mL, until reaching 0 mT. In an alternative approach, the elution and the gradient mode were combined: the process started with a flow rate of 1.2 mL/min and a magnetic flux density of 50 mT, which was then stepwise reduced by 2.5 mT until it reached a certain flux density (20 or 25 mT, respectively) at the end of this process step. Subsequently, the magnetic field was switched off while simultaneously increasing the flow rate to 5 mL/min, thus enabling the targeted release of temporarily bound species. Throughout the studies, the slope and shape of the gradient were iteratively optimized with the aim of maximizing process performance in terms of purities and recoveries.

4. FRACTIONATION RESULTS AND DISCUSSION

4.1. Retardation of Pure Lamp Phosphor Species.

Recent investigations have shown that the removal dynamics of paramagnetic phosphors in an HGMS system are dependent on the intrinsic magnetic susceptibilities of the materials.[28−30] To investigate the retardation behavior of the phosphors within the magnetic field-controlled chromatography column employed in this work, proof-of-concept experiments were conducted using pure suspended phosphors. Three different chromatography operation modes (isocratic, elution, and step gradient, refer to Section 3) were compared with each other. In the isocratic and gradient mode runs, the flow rate was set to 1.2 mL/min, which corresponds to a column residence time of 108 s and kept constant. In the elution mode, the flow rate was initially set to 1.2 mL/min but was increased to 5 mL/min after the appearance of the first UV peak. The chromatograms resulting from the experiments are shown in Figure 3.

The chromatograms revealed that the phosphors were observed to be retarded or even completely retained within the column compared to those in the diamagnetic silica tracer. Retention volumes increased with an increasing magnetic susceptibility. DLS analyses have shown that the particle size distributions of the phosphors matched to a high degree (refer to SI, Figure S2), implying that the divergences in retention volumes were not rooted in the collective's particle sizes but in the inherent differences in their magnetic susceptibilities.

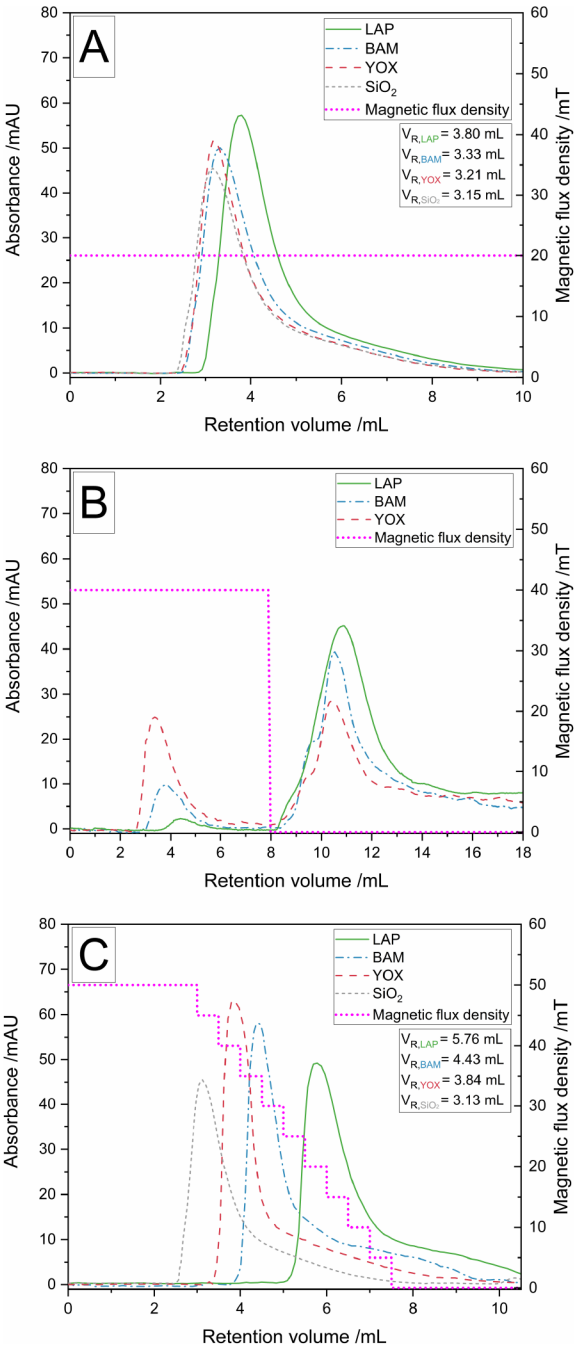

Figure 3. Chromatograms of the pure lamp phosphor (LAP, BAM, and YOX) and silica species retardation experiments. The UV absorbances at 280 nm were measured throughout the experiments. (A) Isocratic operation mode; the magnetic flux density was kept constant at 20 mT throughout the experiment. The characteristic retention volumes $V_{R,i}$ were derived from the chromatogram and are given within the graph. (B) Elution mode, the magnetic flux density was initially set to 40 mT and then the field source was switched off, while simultaneously increasing the flow rate. (C) Step gradient mode, the magnetic field was reduced stepwise from 50 mT until reaching 0 mT. Again, the retention volumes $V_{R,i}$ were determined and are given within the graph.

In the elution mode (Figure 3B), distinct phosphor amounts were retained within the column until elution, depending on the magnetic susceptibility. LAP was found to be more strongly retained than BAM, and YOX showed the weakest retention

among the three phosphors. This suggests that more intense magnetic interactions were present in the first part of the experiment for LAP ($\chi = 3.69 \times 10^{-3}$) than for BAM ($\chi = 1.19 \times 10^{-3}$) and YOX ($\chi = 0.52 \times 10^{-3}$). The elution mode, however, enables effective separation of only two differing species in one processing step, and thus it does not provide any significant advantages over common HGMS methods. Therefore, the elution mode is not the preferred approach for effectively fractionating multicomponent mixtures as aimed for within this work.

The chromatogram obtained under isocratic conditions (Figure 3A) shows that the phosphors were selectively retarded within the column, leading to distinct retention volumes based on their magnetic susceptibilities. Due to its relatively high susceptibility, LAP is more strongly influenced and exhibits the highest retention volume (2.85 mL). However, only slight variations in retention volumes were detected (2.45 mL for BAM, 2.37 mL for YOX, and 2.19 mL for SiO_2), posing a significant challenge for the separation of the three paramagnetic components from the diamagnetic SiO_2. Nevertheless, the differences in retention volumes were enhanced by adapting the operation mode to a temporal magnetic field gradient mode (Figure 3C). For instance, the retention volume of the LAP was increased by a corresponding retention time of 107 s.

The separation effect is governed by the degree of magnetization of the addressed particles. The paramagnetic nature of the phosphors enables the magnetic manipulation of their retention times within the chromatography column. The influence of the external magnetic field is further amplified by placing a ferromagnetic matrix within the column, which generates well-defined field gradients that allow the particles to be affected based on their intrinsic magnetic properties. The higher the magnetic susceptibility of the particles, the stronger the magnetic interaction with the matrix material, leading to a stronger retention and longer retention times. The results suggest that the specific magnetization of the particles combined with the gradient operation can be used to control the fractionation process, possibly enabling the fractionation of complex mixtures into individual components.

To isolate the distinct phosphors from a mixture with high purity and recovery, it was necessary to make a quantitative statement about the separability of the substances. Since the identification of two individual peaks can be difficult with a strong peak overlap, the peak resolutions R were determined based on the chromatograms of the individual substances (Figure 3), where each peak was assigned to a specific phosphor. The peak resolution R for two analytes i and j was calculated from the difference in retention volumes V_R divided by the sum of peak widths at half height $w_{0.5}$:[43]

$$R = 1.18 \cdot \frac{V_{R,j} - V_{R,i}}{w_{0.5,j} + w_{0.5,i}} \tag{6}$$

A peak resolution of 1.5 indicates baseline separation, whereas a peak resolution of 1.0 would correspond to a peak area overlap of 3% assuming a Gaussian peak shape. The peak resolutions resulting from the chromatograms in Figure 3A and C are given in Table 2.

The use of the gradient operation mode thus clearly allowed for better separation performance. This is evidenced by a significant increase in the peak resolution values, indicating that the respective two peaks were better separated from each other using gradient operation mode. For instance, the peak resolution between LAP and SiO_2 was improved by a factor of 4.4 using a magnetic field step gradient.

Table 2. Peak Resolutions Resulting from Peak Analyses of the Single-Component Experiment (Isocratic Mode and Temporal Magnetic Field Step Gradient Mode) Chromatograms[a]

		component j					
		isocratic mode			step gradient mode		
		LAP	BAM	YOX	LAP	BAM	YOX
component i	BAM	0.23	-	-	0.81	-	-
	YOX	0.30	0.06	-	1.22	0.44	-
	SiO_2	0.34	0.09	0.03	1.51	0.86	0.50

[a]The peak resolution R was calculated by dividing the difference between the retention volumes $V_{R,j}$ and $V_{R,i}$ by the sum of peak widths at half peak height, $w_{0.5}$, see Eq 6.

4.2. Fractionations of Mixtures of Rare Earth-Doped Phosphors. Based on the results of the investigations of the individual phosphors, the elution mode was considered to be unsuitable for separating a three-component mixture. Consequently, only the isocratic mode and temporal magnetic field gradient mode were examined regarding their fractionation performance of the phosphor mixture. The result of the isocratic chromatography experiment is visualized in Figure 4A, and the one of the gradient experiments is shown in Figure 4B. Both charts depict the results of three-component fractionation experiments, with the UV absorbance monitored in-line and concentrations representing each individual phosphor analyzed offline and fraction-wise via fluorimetry.

As already revealed by the experiments with the pure phosphors, the isocratic operation mode provides only minor differences in retention volumes and low peak resolutions (Table 2 and Figure 3A). This was again confirmed by the mixture fractionation experiment (Figure 4A), where no separate peaks could be identified with certainty. Only a minor shoulder was observed on the descending peak front, which may be assigned to retarded LAP according to the findings of the pure substance experiments. In contrast, the gradient experiment (Figure 4B) produced overlapping, but clearly distinguishable peaks. The offline concentration analysis of the collected fractions showed that the first peak can be attributed to YOX, the second to BAM, and the third to LAP. This once again confirms the finding from the pure substance experiments that the peak resolutions could be significantly increased by applying a magnetic field gradient mode compared to the isocratic operation mode. The higher peak resolutions obtained during the gradient mode are expected to provide higher phosphor purities in the collected fractions, which were determined using the offline measured concentrations. By utilizing an optimized cutting strategy for LAP, purity was maximized up to 60.7%. In contrast, the maximum LAP purity achieved in the isocratic mode experiment was only 44.6%. If a cutting strategy is chosen that provides relatively high purity, often a lower recovery must be accepted since most of the injected feed material is discarded in the waste stream. Therefore, irrespective of the process operation mode selected, a compromise between achieving a sufficiently high recovery and obtaining the highest possible purity must be found. Figure 5 illustrates the competition between these two parameters for both process operation modes and each of the three phosphors.

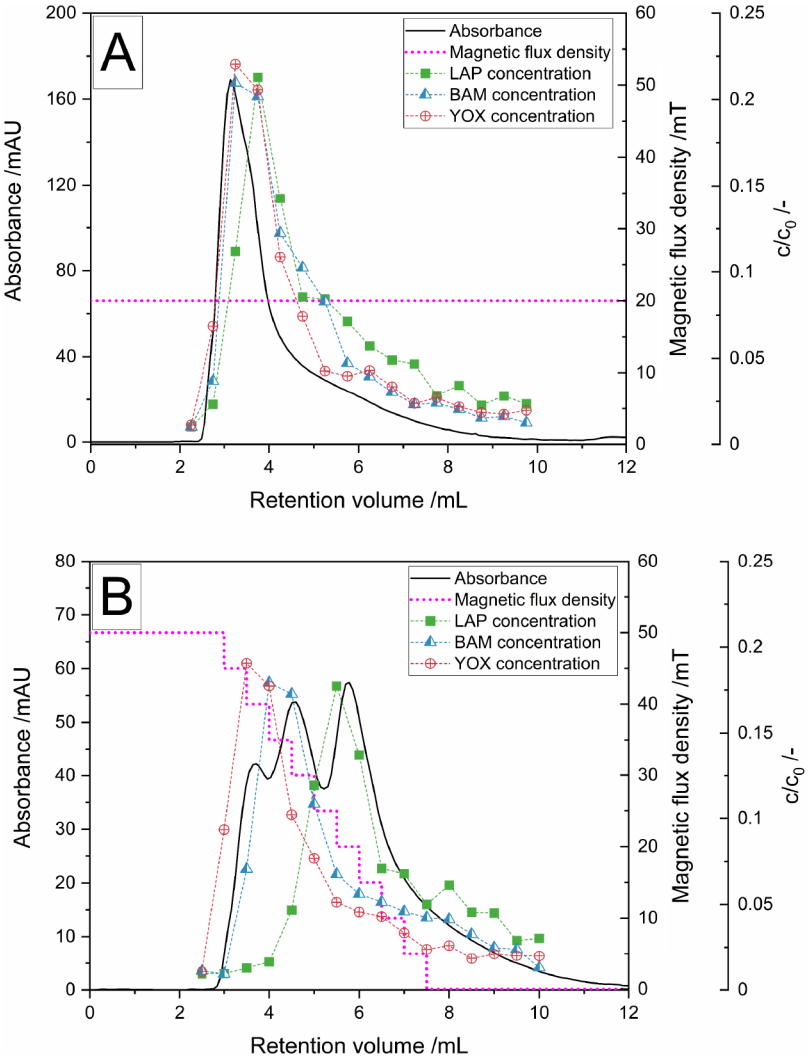

Figure 4. Chromatograms and offline concentration measurement results of the lamp phosphor mixtures. The phosphors LAP, BAM, and YOX were each present in the feed suspension with a concentration of c_i = 0.1 g/L (c_{total} = 0.3 g/L), and the UV absorbance was continuously analyzed at 280 nm over the course of the experiments. Fraction volumes of 0.5 mL were collected at the column outlet and subsequently analyzed offline via fluorimetry for LAP, BAM, and YOX concentrations. The concentrations in the fractions were then normalized to the feed concentration and plotted on the diagram. (A) Isocratic process operation mode and (B) temporal magnetic field gradient mode.

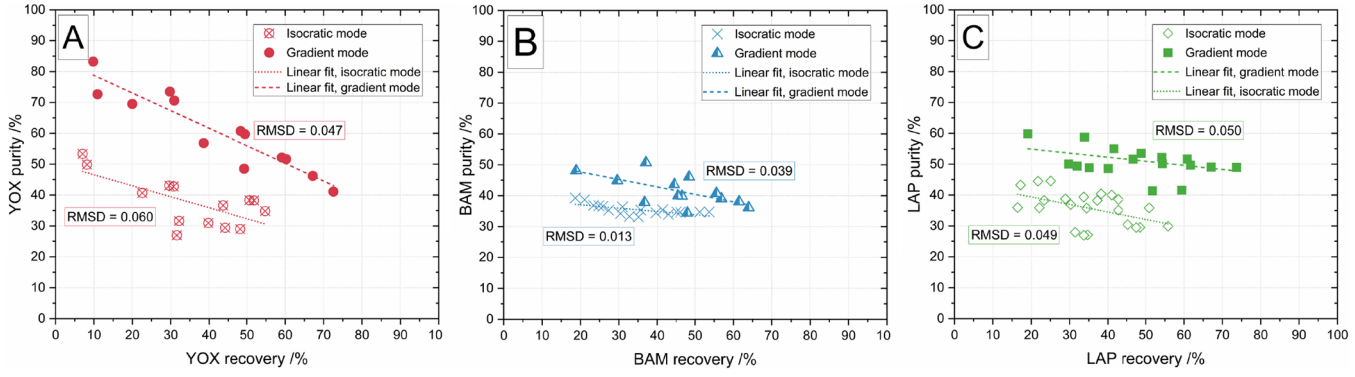

Figure 5. Purity/recovery competition achieved with the isocratic chromatography mode and temporal magnetic field gradient mode for the three different phosphors (A) YOX, (B) BAM, and (C) LAP. Each data point was obtained from different peak cutting strategies. Linear regression was applied for each of the data sets, and the respective root-mean-square deviations (RMSDs) are given within the charts.

The improved peak resolutions observed in the gradient mode (referring to Figure 4B) evidently resulted in a shift of the data pairs toward higher purities and recoveries for each of the three phosphor compounds. This improvement is particularly evident for YOX, with a maximum purity of 83.2% achieved in the gradient experiment (Figure 5A). The

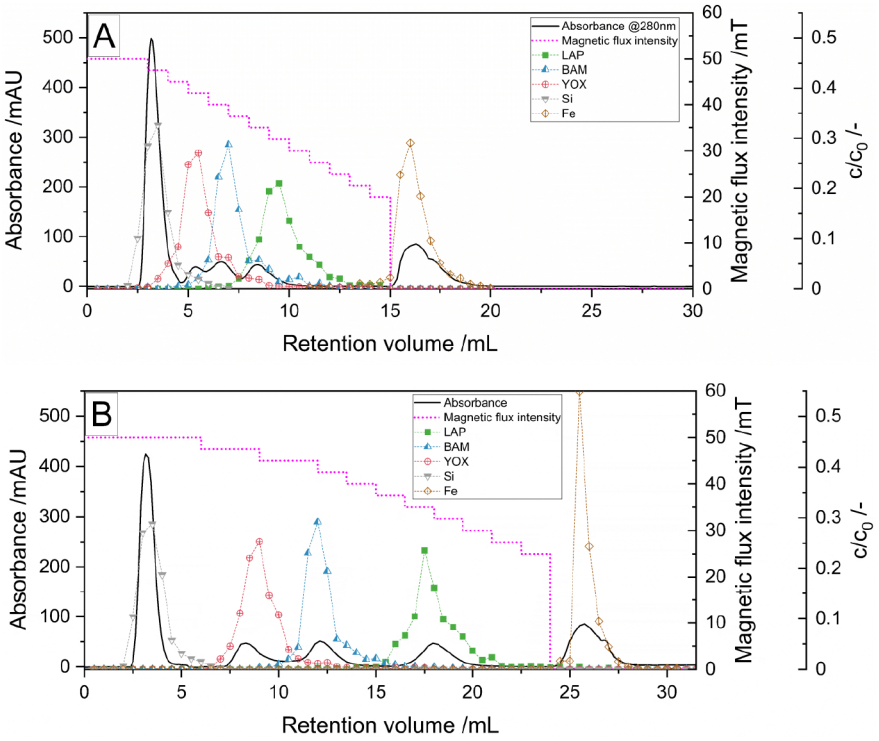

Figure 6. Chromatograms and offline analyzed concentrations of the fractions resulting from magnetic chromatography fractionation processes of the artificial EOL product mixture using combinations of elution and step gradient modes. The phosphors LAP, BAM, and YOX were each present in the feed mixture with a concentration of c_i = 0.09 g/L, the SiO_2 nanoparticle concentration was 13.2 g/L, and the iron oxide nanoparticle concentration was 0.75 g/L. The UV absorbance was continuously analyzed at 280 nm. Fraction volumes of 0.5 mL were collected and subsequently analyzed offline via fluorimetry for LAP, BAM, as well as YOX concentrations and via ICP-OES for Si and Fe contents. The concentrations were normalized to the feed concentrations and plotted on the diagram. (A) Gradient operation mode with a magnetic field reduction of 2.5 mT/mL and an elution step from 20 to 0 mT. (B) Optimized gradient operation mode with changing magnetic field reduction rates (2.5 mT every 3 mL and afterward 2.5 mT every 1.5 mL). As soon as 25 mT was reached, the external magnetic field was switched off.

increases in both purity and recovery for BAM (Figure 5B) and LAP (Figure 5C) were observed to be lower. The purity of BAM is negatively impacted by the fact that the fractions collected at the outlet were being polluted on both the ascending (by YOX) and descending (by LAP) peak fronts. On the other hand, the purity of LAP is restricted because the peaks display a fairly strong tailing, as observed for the pure substances (see Figure 3), leading to the presence of YOX and BAM in the outlet stream long after the peak maxima have occurred. This phenomenon, furthermore, results in a substantial decrease in the recoveries of each of the components.

Additionally, it has been observed that pursuing high purities inevitably leads to lower recoveries, as the descending linear regression curves (see Figure 5, dotted/dashed lines) indicate that these two parameters are inversely related. Therefore, the competition between purity and recovery is an important aspect to consider during process development and optimization. To mitigate this competition, the cutting strategy can be optimized to achieve an optimal balance between purity and recovery. Optimizing the process parameters, for instance by applying a shallower gradient slope may also be beneficial in further enhancing the peak resolutions.

In brief, the findings indicate that the temporal magnetic field gradient mode is a promising approach to enhance fractionation process performance, resulting in improved phosphor purity and recovery compared with the isocratic mode. Nevertheless, further optimization efforts are required to achieve recoveries and purities that are relevant to industrial applications.

4.3. Fractionation of an Artificial End-of-Life Product Mixture. So far, fractionation processes of different phosphor mixtures, specifically those consisting of LAP, BAM, and YOX, were investigated within this study. To further enhance the practical applicability of the process, the fractionation of an artificial EOL product mixture was explored, which comprised the three phosphors, along with two common impurities, silica (SiO_2) and iron oxide in the form of magnetite, at relevant and realistic concentrations. The inclusion of these impurities made the feed mixture more representative of real-world scenarios as they are commonly found in ground EOL fluorescent lamps. Based on the specifications by Binnemans et al. for the composition of ground EOL lamp waste,[12] an artificial EOL product mixture was assembled comprising diamagnetic silica at 13.2 g/L, ferrimagnetic magnetite at 0.75 g/L, and paramagnetic LAP, BAM, and YOX at 0.09 g/L each. As a result, the amount of RE-containing phosphors, constituting 1.9%(w/w), makes up a greater percentage than indicated in the composition stated in the publication by Binnemans et al. (0.3 to 0.6%(w/w)), which was due to the detection limit of the FI analysis method. However, the approach employed in this study mainly relies on a step gradient elution after binding. Thus, applying elevated phosphor concentrations served as a worst-case scenario. If the capacity of the chromatography column is found to be sufficient to achieve a satisfactory fractionation result under these high-load conditions, it may

Table 3. Peak Resolutions Resulting from Peak Analyses of the Use Case Mixture Experiment with the Two Different Magnetic Field Gradient Shapes[a]

		component *j*							
		step gradient				optimized step gradient			
		iron oxide	LAP	BAM	YOX	iron oxide	LAP	BAM	YOX
component *i*	LAP	2.80	-	-	-	2.40	-	-	-
	BAM	3.39	0.75	-	-	4.58	2.14	-	-
	YOX	4.28	1.47	0.61	-	6.00	3.61	1.57	-
	SiO_2	5.61	2.82	1.84	1.37	9.28	6.73	4.61	2.76

[a]The peak resolution R was calculated by dividing the difference between the retention volumes $V_{R,j}$ and $V_{R,i}$ by the sum of peak widths at half peak height $w_{0.5}$, see Eq 6

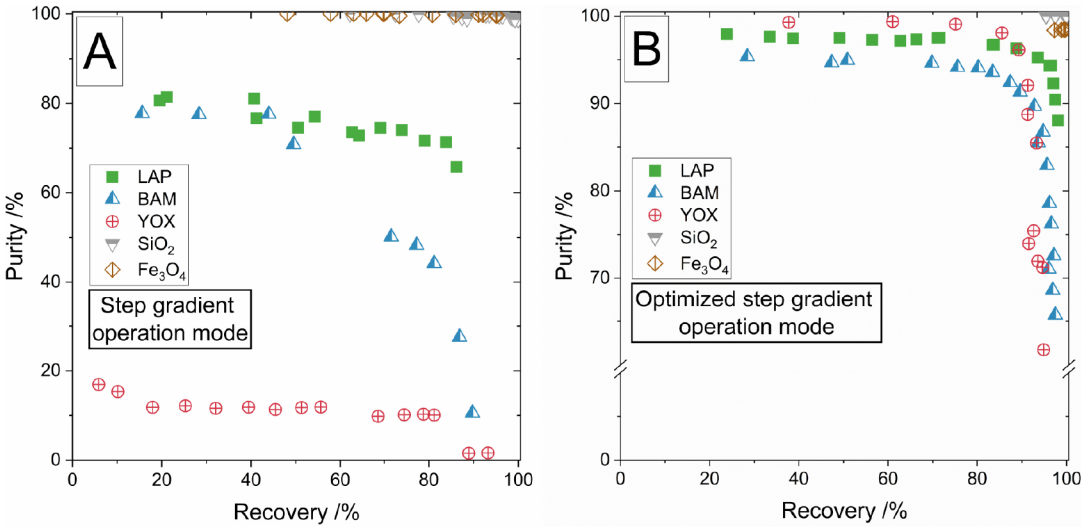

Figure 7. Purity/recovery competition for LAP, BAM, YOX, silica, and iron oxide was achieved with the two different step gradient shapes applied during the chromatography fractionation experiments. (A) Step gradient operation mode with a magnetic field reduction rate of 2.5 mT/mL; refer to figure 6. (B) Optimized gradient shape, refer to figure 6.

reasonably be assumed that this would be the case for lower phosphor concentrations as well.

Two different gradient shapes were investigated. Figure 6 displays the resulting chromatograms as well as offline concentration determinations by FI. The first gradient shape corresponds to the gradient that was already used in the three-component phosphor fractionation experiments. The second gradient shape represents an optimization of the first section of the gradient, representing magnetic flux densities between 50 and 40 mT.

Figure 6A displays the chromatogram resulting from a reduction in magnetic flux density of 2.5 mT/mL and a subsequent elution step from 20 to 0 mT. It can be observed that five distinguishable peaks were obtained, albeit exhibiting a significant overlap of the first four peaks. The offline concentration determinations facilitate clear attribution of the peaks to silica, LAP, BAM, YOX, and iron. During the gradient phase, the dia- and paramagnetic components elute, while the iron-containing peak appears only after switching off the external magnetic field. This suggests that the iron oxide particles were temporarily bound to the matrix surface and were only released upon reducing the external magnetic influence. The first peak containing silica particles appears after a retention volume of 3.16 mL in both chromatograms in Figure 6, which is well comparable to the retention volumes from the single-component experiments (3.13 and 3.15 mL, referring to Figure 3). This confirms that no magnetic interactions occur between the magnetized matrix and the diamagnetic particles that would affect the retention volume, as expected. The paramagnetic phosphors LAP, BAM, and YOX appear slightly offset in the order of increasing magnetic susceptibility during the magnetic field reduction phase. Since the magnetic susceptibilities of YOX and BAM are quite similar, they appear relatively close to each other in the chromatogram ($V_{R,YOX}$ = 5.36 mL, $V_{R,BAM}$ = 6.64 mL), while the LAP peak ($V_{R,LAP}$ = 8.42 mL) appears more separated. This also reflects in the peak resolutions (see Table 3, left); while baseline separation was obtained for the separation of iron oxide from para- and diamagnetic components, this was not possible for the separation of the phosphors from each other. Nevertheless, almost baseline separation could be achieved for LAP/YOX (R = 1.47). The situation changes significantly when the peak resolutions resulting from the optimized gradient are examined (Figure 6B). The optimization in terms of the decreased slope of the temporal magnetic field gradient at the beginning of the experiment clearly enhances the resolution of the peaks of the paramagnetic components. This benefit comes at the expense of an extended duration of the process, and thus higher eluent consumption. For each of the component pairs, a resolution >1.5 was obtained (see Table 3, right-hand side), however, it must be taken into account that the assumption of Gaussian-shaped peaks is not given in each case (particularly for the second and third peak, YOX/BAM, in Figure 6B). We hypothesize that the significant

tailing behavior observed for the elution peaks of these components is rooted in the polydispersity of the particle collectives. Since the magnetic force is based on the particle volume, the smallest particles in the collective travel through the column with a higher velocity as the magnetic flux intensity gradually decreases during gradient elution, while the largest particles remain bound at specific sites. This will result in severe peak broadening, as observed in Figure 6B.

After analyzing the purity/recovery relationships depicted in Figure 7A for the first gradient shape and in Figure 7B for the optimized, second gradient shape, it is evident that optimizing the gradient can lead to a substantial enhancement in separation performance while also maintaining or even boosting the recovery (note the broken purity axis in Figure 7B). The fractions rich in YOX, which were previously heavily polluted with silica particles, now exhibit purities of up to 99.1% while retaining a recovery of more than 75.1%. Additionally, the LAP-rich fractions exhibit significantly higher purities than before (97.9% versus 81.4%). The BAM fractions are found to deliver the least favorable purity/recovery value pairs (purities of up to 95.3%). Overall, by optimizing the magnetic field gradient, process performance may be significantly enhanced while recovery is maintained or even increased. Higher purities for BAM may require a second, serially connected processing step at the expense of a decrease in recovery; however, the achieved purities have not previously been reported in the literature.

5. CONCLUSION AND OUTLOOK

The aim of this work was to design a process for the fractionation of three different RE-containing phosphors used in fluorescent lamps. The retardation behavior of the lamp phosphors within a magnetizable chromatography column under the influence of an ambient magnetic field was studied extensively. Initially, proof-of-concept experiments were conducted using pure phosphor species to compare three different chromatography operation modes. The results suggest that the phosphors were significantly retarded or even retained within the column compared with the diamagnetic silica particle tracer. The particle−matrix affinity was found to intensify with higher magnetic susceptibility, with some phosphors being entirely retained within the column at specific magnetic flux densities. The elution mode allowed for the separation of only two differing species in a single processing step (similar to HGMS), and the isocratic mode posed a significant challenge because of only slight differences in retention volumes. However, the retention volumes could be significantly enhanced by adapting the operation mode to a temporal magnetic field step gradient mode, indicating that the specific magnetization of the particles combined with a careful choice of the process parameters can be used to control the separation outcome. We further investigated the fractionation of mixtures of RE-doped phosphors as well as an artificial EOL product mixture consisting of five components at realistic concentrations. The results demonstrate that magnetic chromatography is capable of separating particles below 10 μm based not only on their differing magnetic properties (such as dia-, para-, and ferrimagnetism) but also on their intrinsic magnetic susceptibilities in the case of paramagnetic behavior. Again, the peak resolutions were significantly improved by optimizing the gradient shape, which resulted in a purity of 95.3% while maintaining a recovery of 93.6% in the case of LAP. The promotion of RE-containing EOL product recycling, which is primarily motivated by environmental concerns and resource conservation, also requires examination of other relevant key parameters. In this context, the pursuit of ecologically friendly and cost-effective fractionation technologies has gained traction. Thus, it is highlighted that all fractionation experiments in this work were performed in aqueous systems containing only a minimal portion of a nontoxic and biodegradable organic solvent (20%(v/v) ethanol). The eluent consumption demonstrated a commendable level of efficiency, with a consumption rate of only 4.1 L/(g) of particle feed mass. Notably, the eluent composition remained unchanged throughout the process, reflecting a nonchemical elution method. The findings of this study therefore highlight the potential of magnetic field-controlled chromatography, which may contribute to the development of more efficient and effective purification methods for the recycling of RE-containing EOL products. While further effort is needed to scale up the proposed method for industrial application, the possibility of increasing the column size and/or applying continuous chromatography methods (as shown for the fractionation of superparamagnetic nanoparticle collectives in a previous work[44]) underscores its practicality and applicability.

AUTHOR INFORMATION

Corresponding Author

Laura Kuger − *Institute for Functional Interfaces (IFG), Karlsruhe Institute of Technology, Eggenstein-Leopoldshafen 76344, Germany;* orcid.org/0000-0001-7323-1158; Email: laura.kuger@kit.edu

Author

Matthias Franzreb − *Institute for Functional Interfaces (IFG), Karlsruhe Institute of Technology, Eggenstein-Leopoldshafen 76344, Germany;* orcid.org/0000-0003-3586-4215

Notes

The authors declare no competing financial interest.

ACKNOWLEDGMENTS

The authors gratefully acknowledge the financial support of the Deutsche Forschungsgemeinschaft (DFG). The work was done within the priority project SPP2045, subproject C11 (grant number FR 2131/6−2). Furthermore, the authors thank Marita Heinle and Peter Weidler from KIT for performing the ICP-OES and XRD analyses, as well as the companies

micromod Partikeltechnologie GmbH and Leuchtstoffwerk Breitungen GmbH for kindly providing particle material for the experiments.

ADDITIONAL NOTE

[a]Assuming that the magnetic susceptibility of the paramagnetic particle significantly exceeds the volume susceptibility of the surrounding liquid: $\chi \gg \chi_l$.

REFERENCES

(1) Gupta, C. K.; Krishnamurthy, N. *Extractive metallurgy of rare earths*; CRC Press: Boca Raton, FL, USA, 2005.
(2) Wang, S.; Hausfather, Z.; Davis, S.; Lloyd, J.; Olson, E. B.; Liebermann, L.; Núñez-Mujica, G. D.; McBride, J. Future demand for electricity generation materials under different climate mitigation scenarios. *Joule* **2023**, *7* (2), 309−332.
(3) Baldi, L.; Peri, M.; Vandone, D. Clean energy industries and rare earth materials: Economic and financial issues. *Energy Policy* **2014**, *66*, 53−61.
(4) Binnemans, K.; Jones, P. T.; van Acker, K.; Blanpain, B.; Mishra, B.; Apelian, D. Rare-Earth Economics: The Balance Problem. *JOM* **2013**, *65* (7), 846−848.
(5) U.S. Department of Energy. *Critical Minerals and Materials: U.S. department of energy's strategy to support domestic critical mineral and material supply chains*; U.S. Department of Energy, 2021.
(6) U.S. Geological Survey. *Mineral Commodity Summaries*; U.S. Geological Survey, 2021.
(7) European Commission. Communication from the Commission to the European Parliament, the Council, the European Economic and Social Committee and the Committee of the Regions. Critical Raw Materials Resilience: Charting a Path towards greater Security and Sustainability; European Commission: Brussels, 2020; Vol. *474*.
(8) Mancheri, N. A.; Sprecher, B.; Bailey, G.; Ge, J.; Tukker, A. Effect of Chinese policies on rare earth supply chain resilience. *Resour., Conserv. Recycl.* **2019**, *142*, 101−112.
(9) Liang, T.; Li, K.; Wang, L. State of rare earth elements in different environmental components in mining areas of China. *Environ. Monit. Assess.* **2014**, *186* (3), 1499−1513.
(10) Binnemans, K.; Jones, P. T.; Blanpain, B.; et al.et al. Recycling of rare earths: A critical review. *J. Cleaner Prod.* **2013**, *51*, 1−22.
(11) Reck, B. K.; Graedel, T. E. Challenges in Metal Recycling. *Science* **2012**, *337*, 690−695.
(12) Binnemans, K.; Jones, P. T. Perspectives for the recovery of rare earths from end-of-life fluorescent lamps. *J. Rare Earths* **2014**, *32* (3), 195−200.
(13) Graedel, T. E.; Allwood, J.; Birat, J.-P.; et al.et al. What Do We Know About Metal Recycling Rates? *J. Ind. Ecol.* **2011**, *15* (3), 355−366.
(14) Rhee, S.-W.; Choi, H.-J. Evaluation on Recovery of Glass and Plastics from Compact Fluorescent Lamps (CFLs) by Air Separation Unit. *Eng. J.* **2016**, *20* (4), 121−127.
(15) Kelly, E. G.; Spottiswood, D. J. The theory of electrostatic separations: A review Part I. Fundamentals. *Miner. Eng.* **1989**, *2* (1), 33−46.
(16) Higashiyama, Y.; Asano, K. Recent Progress in Electrostatic Separation Technology. *Part. Sci. Technol.* **1998**, *16* (1), 77−90.
(17) Pope, M. I.; Sutton, D. I. The correlation between froth flotation response and collector adsorption from aqueous solution. Part I. Titanium dioxide and ferric oxide conditioned in oleate solutions. *Powder Technol.* **1973**, *7* (5), 271−279.
(18) Cheng, T. W. The Point of Zero Charge of Monazite and Xenotime. *Miner. Eng.* **2000**, *13* (1), 105−109.
(19) Hirajima, T.; Bissombolo, A.; Sasaki, K.; Nakayama, K.; Hirai, H.; Tsunekawa, M. Floatability of rare earth phosphors from waste fluorescent lamps. *Int. J. Miner. Process.* **2005**, *77* (4), 187−198.
(20) Otsuki, A.; Dodbiba, G.; Fujita, T. Separation of a mixture of rare earth fluorescent powders by two-liquid flotation using polar and non-polar organic solvents for recycling. In *Digest Of Papers Microprocesses And Nanotechnology*; IEEE, 2007; pp 236237.
(21) Otsuki, A.; Dodbiba, G.; Shibayama, A.; Sadaki, J.; Mei, G.; Fujita, T. Separation of Rare Earth Fluorescent Powders by Two-Liquid Flotation using Organic Solvents. *Jpn. J. Appl. Phys.* **2008**, *47* (6), 5093−5099.
(22) Mei, G.; Rao, P.; Mitsuaki, M.; Toyohisa, F. Separation of red (Y_2O_3: Eu^{3+}), blue (Sr, Ca, Ba)$_{10}$(PO_4)$_6$$Cl_2$: Eu^{2+} and green ($LaPO_4$: Tb^{3+}, Ce^{3+}) rare earth phosphors by liquid/liquid extraction. *J. Wuhan Univ. Technol., Mater. Sci. Ed.* **2009**, *24* (3), 418−423.
(23) Wada, K.; Mishima, F.; Akiyama, Y.; Nishijima, S. The Development of the Separation Apparatus of Phosphor by Controlling the Magnetic Force. *Phys. Procedia* **2014**, *58*, 252−255.
(24) Wankat, P. C.; Hwang, J. Y.; Beckemeyer, D.; Friedlaender, F. Removal of Paramagnetic Particles from Single Wire HGMS. *IEEE Trans. Magn.* **1984**, *20* (5), 1177−1179.
(25) Gerber, R.; Birss, R. R. *High Gradient Magnetic Separation*; Research Studies Press: Baldock, UK, 1983.
(26) Gerber, R.; Takayasu, M.; Friedlaender, F. Generalization of HGMS theory: The capture of ultra-fine particles. *IEEE Trans. Magn.* **1983**, *19* (5), 2115−2117.
(27) Oberteuffer, J. High Gradient Magnetic Separation. *IEEE Trans. Magn.* **1973**, *9* (3), 303−306.
(28) Yamashita, M.; Akai, T.; Murakami, M.; Oki, T. Recovery of LaPO4: Ce,Tb from waste phosphors using high-gradient magnetic separation. *Waste Manage.* **2018**, *79*, 164−168.
(29) Yamashita, M.; Akai, T.; Imamura, T.; Murakami, M.; Oki, T. Recycling of waste phosphors using high gradient magnetic separation method. *Trans. Mater. Res. Soc. Jpn.* **2014**, *39* (1), 35−37.
(30) Boelens, P.; Lei, Z.; Drobot, B.; et al.et al. High-Gradient Magnetic Separation of Compact Fluorescent Lamp Phosphors: Elucidation of the Removal Dynamics in a Rotary Permanent Magnet Separator. *Minerals* **2021**, *11*, 1116.
(31) Schunk, T. C.; Gorse, J.; Burke, M. F. Parameters Affecting Magnetic Field-Flow Fractionation of Metal Oxide Particles. *Sep. Sci. Technol.* **1984**, *19* (10), 653−666.
(32) Gorse, J.; Schunk, T. C.; Burke, M. F. The Study of Liquid Suspensions of Iron Oxide Particles with a Magnetic Field-Flow Fractionation Device. *Sep. Sci. Technol.* **1984**, *19* (13−15), 1073−1085.
(33) Tsukamoto, O.; Ohizumi, T.; Ohara, T.; Mori, S.; Wada, Y. Feasibility study on separation of several tens nanometer scale particles by magnetic field-flow-fractionation technique using superconducting magnet. *IEEE Trans. Appl. Supercond.* **1995**, *5* (2), 311−314.
(34) Ohara, T.; Mori, S.; Oda, Y.; Wada, Y.; Tsukamoto, O. Feasibility of Magnetic Chromatography for Ultra-Fine Particle Separation. *IEEJ Trans. Power Energy* **1996**, *116* (8), 979−986.
(35) Mitsuhashi, K.; Yoshizaki, R.; Ohara, T.; Matsumoto, F.; Nagai, H.; Wada, H. Retention of ions in a magnetic chromatograph using high-intensity and high-gradient magnetic fields. *Sep. Sci. Technol.* **2002**, *37* (16), 3635−3645.
(36) Karki, K. C.; Whitby, E. R.; Patankar, S. V.; Winstead, C.; Ohara, T.; Wang, X. A numerical model for magnetic chromatography. *Appl. Math. Modell.* **2001**, *25* (5), 355−373.
(37) Kelland, D. R. Magnetic separation of nanoparticles. *IEEE Trans. Magn.* **1998**, *34* (4), 2123−2125.
(38) Stieß, M. *Mechanische Verfahrenstechnik - Partikeltechnologie 1*, 3rd ed.; Springer Berlin Heidelberg: Berlin, Heidelberg, 2009.
(39) Watson, J. High Gradient Magnetic Separation. In *Solid−Liquid Separation*, Svarovsky, L., Ed.; Butterworths, 1990; pp 661684.
(40) Visser, J. Van der Waals and Other Cohesive Forces Affecting Powder Fluidization. *Powder Technol.* **1989**, *58*, 1−10.
(41) Wingo, R. M.; Prenger, F. C.; Johnson, M. D.; Waynert, J. A.; Worl, L. A.; Ying, T. High-Gradient Magnetic Field Split-Flow Thin Channel (HGMF-SPLITT) Fractionation of Nanoscale Paramagnetic Particles. *Sep. Sci. Technol.* **2004**, *39* (12), 2769−2783.

(42) Kotz, F.; Risch, P.; Helmer, D.; Rapp, B. E. Highly Fluorinated Methacrylates for Optical 3D Printing of Microfluidic Devices. *Micromachines* **2018**, *9* (3), 115.
(43) Seidel-Morgenstern, A.; Schulte, M.; Epping, A. Fundamentals and General Terminology. In *Preparative Chromatography. Second, Completely Revised and Updated*; Schmidt-Traub, H.; Schulte, M.; Seidel-Morgenstern, A., Eds.; Wiley-VCH Verlag & Co. KGaA: Weinheim, Germany, 2012.
(44) Kuger, L.; Arlt, C.-R.; Franzreb, M. Magnetic/flow controlled continuous size fractionation of magnetic nanoparticles using simulated moving bed chromatography. *Talanta* **2022**, *240*, 123160.